Solid Freeform Fabrication 2021: Proceedings of the 32nd Annual International
Solid Freeform Fabrication Symposium – An Additive Manufacturing Conference
Reviewed Paper

Locational dependency of additively manufactured parts: effects of surface roughness on fatigue behavior

Seungjong Lee[1,2], Muztahid Muhammad[1,2], Jingyi Zheng[3], Shuai Shao[1,2], Nima Shamsaei[1,2*]

[1] Department of Mechanical Engineering, Auburn University, Auburn, AL 36849, USA
[2] National Center for Additive Manufacturing Excellence (NCAME), Auburn University, Auburn, AL 36849, USA
[3] Department of Mathematics and Statistics, Auburn University, Auburn, AL 36849, USA

*Corresponding Author:
Email: shamsaei@auburn.edu
Phone: (334) 844 4839

Abstract

Surface roughness (SR) can vary significantly among parts manufacutred at different locations on the same build platform because of the gas flow and powder recoating process in current laser beam powder bed fusion (LB-PBF) technique. In this study, intra-build SR variation across locations was investigated for LB-PBF 316L stainless steel. The build platform was divided into 4 quadrants to assess the location-dependent variation of SR. Uniaxial stress-controlled fatigue tests were conducted using a servo-hydraulic system. The SR from the four quadrants was analyzed using the one-way Analysis of Variance (ANOVA) method and further verified SR's location dependency. Kruskal-Wallis test was also employed since Box-Cox transformed data failed to meet the requirements of the ANOVA test. Kruskal-Wallis test revealed that there are statistically significant differences in SR values across different locations. The results were validated using fatigue test results and gas flow simulation results reported in literature.

Keywords: Additive manufacturing (AM); Laser beam powder bed fusion (LB-PBF); Surface roughness; Stainless steel; Fatigue.

Introduction

Additive manufacturing (AM), a "layer-by-layer" manufacturing method, has emerged as a viable option with remarkable advantages [1]. Unlike conventional manufacturing processes, AM has the capability to manufacture parts even with complex geometries in near-net shape with little to no post-processing. Hence, AM methods have an edge over conventional manufacturing methods for producing parts with complex geometries (e.g., lattice or gyroid structure) and customized parts for a biomedical sector (e.g., implants). Laser beam powder bed fusion (LB-PBF) is one of the most used AM techniques where layer of powder is spread over the build platform from powder feedstock prior to melting and deposition of powders utilizing a laser heat source.

In spite of using optimized surface process parameters, this layer by layer and track by track melting and remelting steps of LB-PBF induce higher surface roughness (SR) hence inferior fatigue properties in parts compared to the conventional manufacturing processes [2]. In addition, the SR appears to vary significantly even for parts within the same build at different locations because of the gas flow and powder recoating during fabrication of parts using LB-PBF method [3]. Accordingly, intra-build variation of fatigue lives of specimens can occur [6]. Hence, it is critical to have knowledge regarding the location dependency of surface characteristics and the SR parameters (e.g., maximum depth valley, average arithmetic surface roughness, etc.). For instance, Chen et al. noted that SR was higher for specimens built away from the build platform center using the EOS LB-PBF system [7]. Wen et al. claimed that the surface quality can be deteriorated by the unoptimized gas circulation system in LB-PBF [8], and Parteli and Poschel founded that a strong polydispersity of powder may lead to larger SR as a result of attractive particle interaction forces [9].

Despite the hand of existing research, revealing the effects of different SR parameters on fatigue behavior AM parts is challenging since the parameters are intertwined cannot be independently controlled. In this study, the statistical approach was employed to investigate the final locational dependency of SR using quantitative analysis with profiled SR data. The SR of LB-PBF 316L stainless steel (SS) specimens build from each quadrant (northeast (NE), northwest (NW), southeast (SE), and southwest (SW)) was measured. Moreover, their effects on fatigue performance were also investigated.

Experimental Procedure

The rectangular flat fatigue specimens were designed based on ASTM standard E466 [10], and were fabricated using a Renishaw AM250 LB-PBF metallic AM machine and the 316L SS powder with a particle size of 15-45 μm. In order to best characterize the location dependency, the substrate of the build platform was divided into 4 quadrants: northeast (NE), northwest (NW), southeast (SE), and southwest (SW). Total 9 specimens were fabricated at each location on the

build platform. Figure 1(a) shows the geometry of the specimen, and Figure 1(b) describes the build platform, indicating directions of shielding gas flow and recoating process schematically. The default process parameters recommended by the manufacturer (Renishaw) were utilized to fabricate 316L SS parts (see Table 1). Argon was used as a shielding gas, and the build platform was preheated to 80 °C before fabrication.

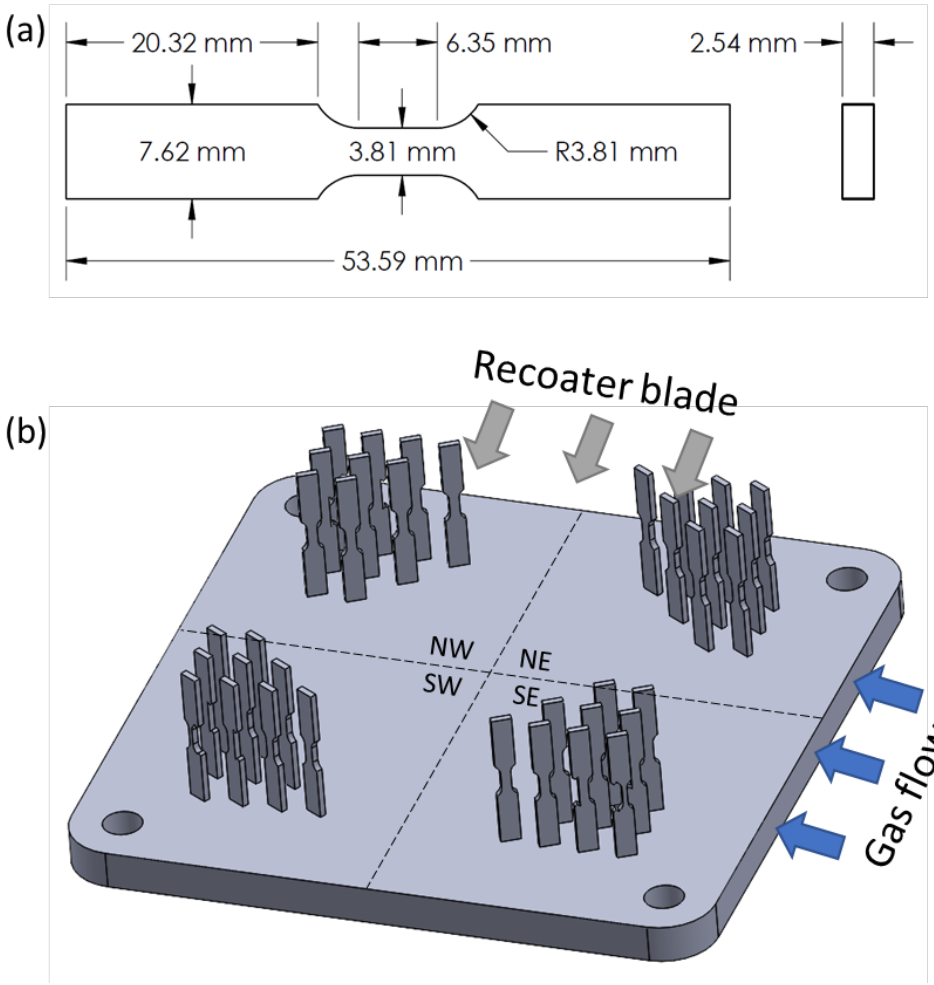

Figure 1 (a) Schematic of net-shape 316 L SS specimens with dimensions, (b) schematic of the build platform including the indications of 4 quadrants and directions of shielding gas flow and recoating process.

Table 1 Process parameters employed to fabricate 316L SS parts.

Laser power	Scan speed	Hatching distance	Layer thickness
200 W	1833.3 mm/sec	110 µm	50 µm

A Keyence VHX-6000 3D digital microscope was used to capture the topological surface images of every specimen. The entire gage section was scanned using a 3D stitching function with a pixel size of 0.43 μm × 0.43 μm at once to obtain the sampling length. Based on the images, height values for each pixel were converted and presented as a CSV file. According to the ISO 4287:2000 [11], 10 line-roughness profiles were extracted from the raw CSV data and the commonly used SR values were calculated using MATLAB. The extracted 10 line-roughness profiles were post-processed for tilt/slope corrections and revised by a Gaussian filter to reduce the possible errors. In total, 360 SR values from 90 profiled lines for each corner were prepared to conduct statistical analyses. The statistical analyses were accomplished using RStudio.

The fully-reversed uniaxial force-controlled fatigue tests were conducted using an MTS landmark servo-hydraulic test frame with a 100 kN capacity load cell based on ASTM E466 [10]. Before fatigue tests, the narrow sides of rectangular specimens were manually polished using abrasive papers to reduce the chance of crack initiations from these locations. The applied force was calculated using the effective area, which does not consider SR as a load-bearing area [6]. Once the fatigue lives reached 5 million cycles, the tests were stopped and considered as run-outs.

Results and Discussion

The mean and standard deviation of standard line-roughness parameters, including arithmetical mean height of the profiled line (R_a), the maximum peak height of the profiled line (R_p), and maximum valley depth of the profiled line (R_v) for each corner were calculated and listed in Table 2. Since R_a represents the arithmetical mean of profiled surfaces and indicates a general texture, it is most commonly used [12,13]. However, it has been observed that R_v is more appropriate SR parameter to represent the effect of surface condition on fatigue behavior since R_v indicates the deepest valley, which can act as a micro-notch on the surface resulted in early crack initiations [14,15]. Therefore, R_v was used as a representative SR parameter in this study to correlate SR with fatigue performance.

Table 2 The mean and standard deviation (STD) of standard line-roughness parameters (R_a, R_p, and R_v) from each quadrant.

Quadrants	R_a (μm)		R_p (μm)		R_v (μm)	
	Mean	STD	Mean	STD	Mean	STD
Northeast (NE)	18.11	4.65	76.01	15.61	49.93	12.86
Northwest (NW)	10.47	1.97	45.82	12.52	31.98	6.14
Southeast (SE)	10.41	4.89	50.89	29.26	28.33	9.87
Southwest (SW)	7.48	1.60	38.91	13.63	19.68	3.91

To analyze the SR dependency on the locations of the build platform, one-way Analysis of Variance (ANOVA) of R_v of each quadrant was performed with the following hypotheses:

H_0: There is no difference in the means of SR of specimens at different locations.

H_a: At least two locations (i.e., one pair of quadrants) have different SR means.

The results of one-way ANOVA were summarized in Table 3. According to the P-value of the ANOVA test, we rejected the null hypothesis and concluded that the means of SR at different locations/quadrants of the build platform are statistically different.

Table 3 ANOVA table regarding 360 profiled R_v.

Source of variations	Degrees of freedom	Sum of squares	Mean squares	F	P-value
Between (quadrants)	3	43708	14569	182.5	$< 2\times10^{-16}$
Within (residuals)	356	28413	80		
Total	359	72121			

To evaluate the ANOVA test and its assumptions (i.e., normality, independency, and homogeneity of variance), we employed some diagnostic tests as shown in Figure 2. Figure 2 (a) indicated that 1) the variances were not equal across locations/quadrants, which violates the variance of homogeneity assumption, 2) there are outliers. In addition, Bartlett's test was conducted, and the P-value ($< 2.2\times10^{-16}$) was much less than 0.05. Therefore, the data did not have equal variance across four locations. The long-tail normal Q-Q plot in Figure 2 (b) implied that the data is skewed. The Shapiro-Wilk normality test also gave a small P-value (5.2×10^{-16}) which is much less than 0.05. According to the Q-Q plot and Shapiro-Wilk test results, the normality was significantly violated.

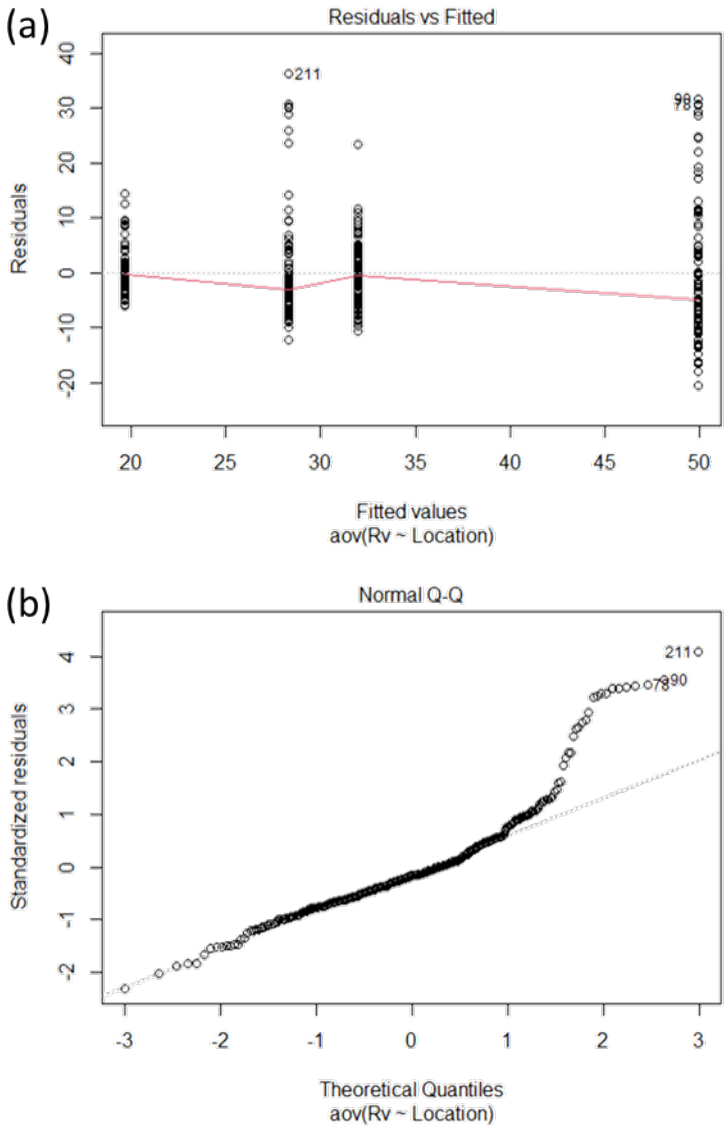

Figure 2 Diagnosis of robustness to assumptions: (a) "Residual vs. Fitted" plot to determine the homogeneity of variances and (b) "Normal Q-Q" plot to determine the normality of residuals.

Though ANOVA is relatively robust to the violation of normality and homogeneity, we applied Box-Cox transformation on the data to satisfy the assumptions. The Box-Cox transformation was conducted using a lambda value of -0.6. Figure 3 shows the boxplots of R_v before (a) and after Box-Cox transformation (b). The one-way ANOVA was conducted again using the transformed data and the results were summarized in Table 4. The null hypothesis was rejected again, which means there are differences in the mean of R_v values at different quadrants of the build platform. The higher R_v of NE specimens may be associated with the velocity of inert gas flow. Flow nozzles of the Renishaw AM 250 system are situated at the eastern side of the build chamber and are situated at a certain height, which creates unstable gas flow at the NE zone; this phenomenon is supported by the literature [3].

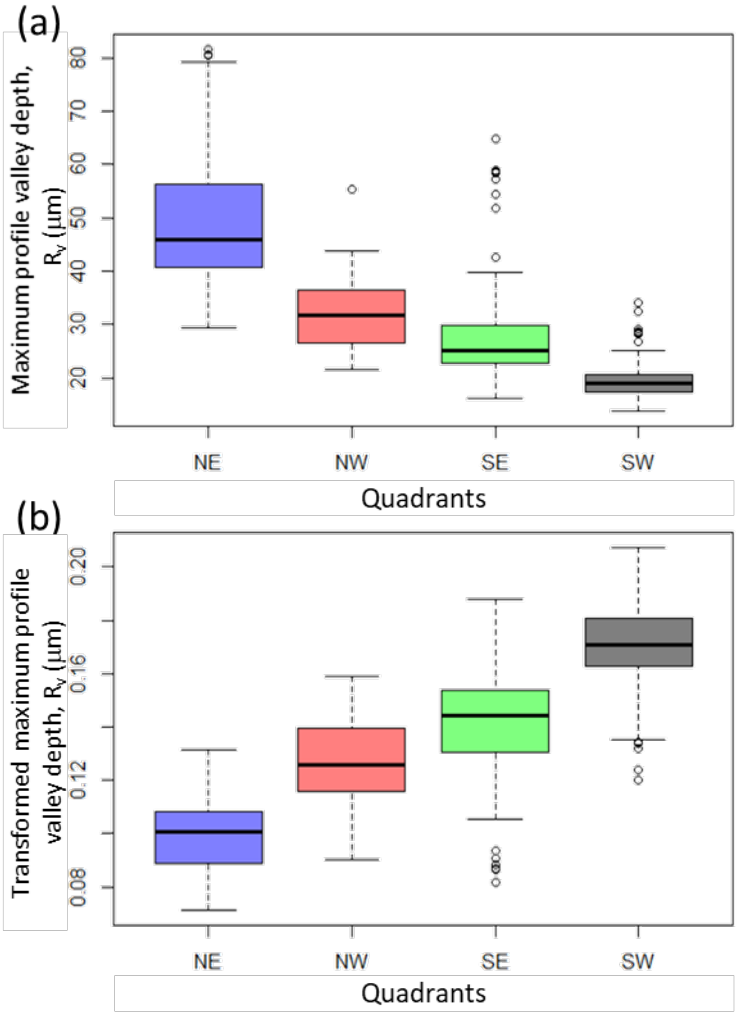

Figure 3 Boxplots of R_v for each quadrant (a) before and (b) after Box-Cox transformation using a lambda value of -0.6.

Table 4 ANOVA table after Box-Cox transformation using a lambda value of -0.6.

Source of variations	Degrees of freedom	Sum of squares	Mean squares	F	P-value
Between (quadrants)	3	0.2378	0.07927	268.8	$< 2\times10^{-16}$
Within (residuals)	356	0.1050	0.00029		
Total	359	0.3428			

Diagnostic analysis was conducted again to check the ANOVA fitting and assumptions as shown in Figure 4. The Bartlett's test (P-value = 7.1×10^{-16}) and Shapiro-Wilk test (P-value = 1.767e-05) provided larger P-values than raw data. However, the P-values are still much less than

0.05. After data transformation, the normality and homogeneity issues were partially addressed but still not well satisfied.

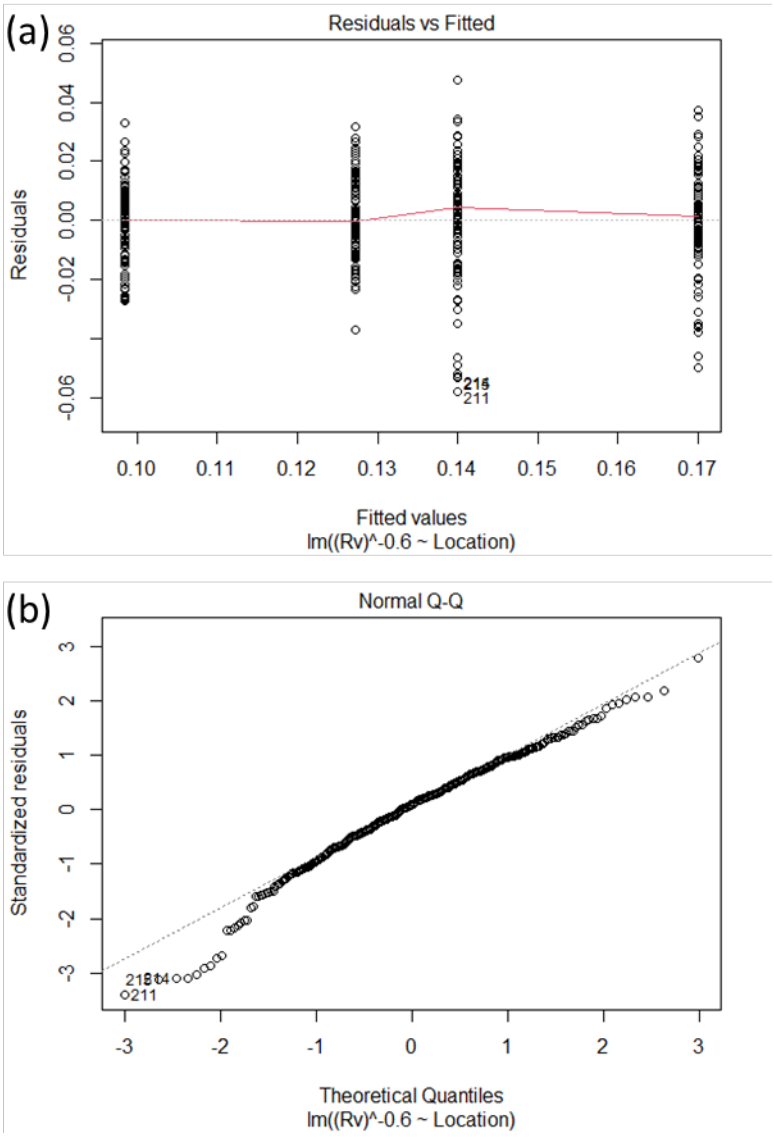

Figure 4 Diagnosis of robustness to assumptions after Box-Cox transformation: (a) "Residual vs. Fitted" plot to determine the homogeneity of variances and (b) "Normal Q-Q" plot to determine the normality of residuals.

Since ANOVA test was robust to the violation of normality and homogeneity of variance, the test results were trustable. But due to the violation of the ANOVA assumption, we also performed the nonparametric Kruskal-Wallis test to make sure the results and our conclusion were statistically valid. According to the test results, the chi-squared was 254.37 and P-value was much less than 0.05 (p-value $< 2.2\times10^{-16}$). Therefore, the null hypothesis was also rejected by the Kruskal-Wallis test. Since we rejected the null hypothesis, a post-hoc test, Tukey-Kramer procedures, were applied to make pairwise comparisons. Table 5 shows the result of applied Tukey-Kramer method and Figure 5 illustrates the pair-wise relationship of R_v among different

quadrants. Both p-values in Table 5 and illustrated pairwise comparisons show that all pairs have differences in their mean. As a result, all statistical analyses indicated that there are differences in the mean of R_v values based on quadrants of the build platform.

Table 5 Tukey-Kramer test results.

Quadrants	differences	lower	upper	P-value
NW-NE	-17.952	-21.3896	-14.5144	0
SE-NE	-21.5986	-25.0362	-18.161	0
SW-NE	-30.2438	-33.6814	-26.8062	0
SE-NW	-3.64659	-7.08416	-0.20901	0.032738
SW-NW	-12.2918	-15.7294	-8.85424	0
SW-SE	-8.64523	-12.0828	-5.20765	0

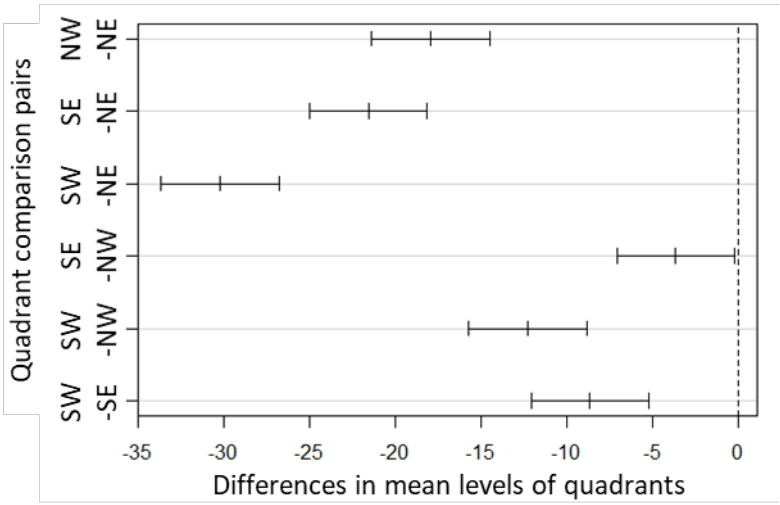

Figure 5 Pair-wise R_v mean comparison between quadrants.

The difference in R_v of each quadrant should reflect in the fatigue performance of specimens from each quadrant as well. The stress-life plot was generated as shown in Figure 6. In the low cycle fatigue (LCF) regime, the fatigue lives of each quadrant are similar, apposing to those in the high cycle fatigue (HCF) regime. In HCF, fatigue performance of specimens from NE quadrants was the worst and followed by NW, SE, and SW, in order. This trend of fatigue performance in terms of specimens from each quadrant correlates with R_v (see Figure 3(a)). It confirmed that specimens from the same build platform can indeed have statistically different SR values, resulting in different fatigue performances.

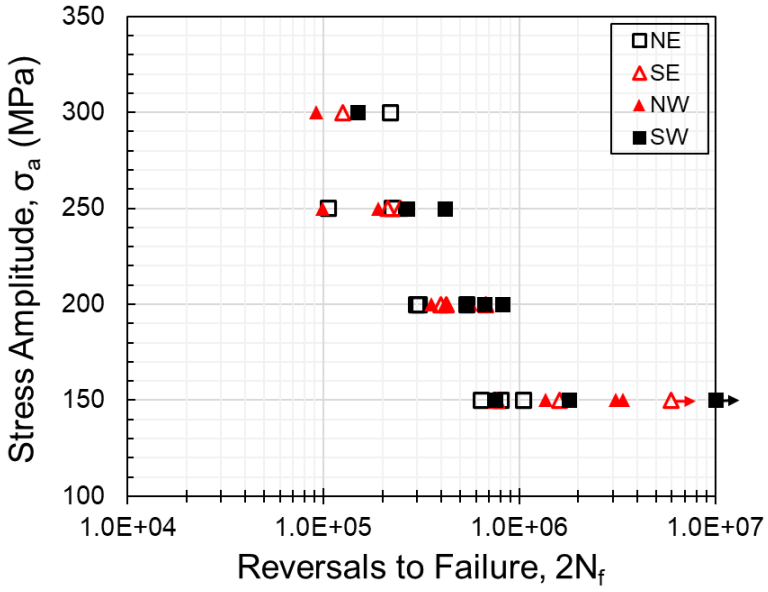

Figure 6 Stress-life plot presenting fatigue behavior of LB-PBF 316L SS fabricated in different build platform locations.

Due to the unique processing and thermal history of AM, an individual part does not necessarily have uniform SR throughout the surface, which was a major challenge towards the requirement to fulfill the assumptions of ANOVA. However, with a larger population of observational data and with the application of a nonparametric approach, it was confirmed that there is indeed variation in the SR of additive manufactured parts based on the location of the build platform. According to R_v values, the NE zone provides the highest SR values and the SW zone provides the lowest SR values. These results are matched with simulated velocity contour from the literature [3]. The quadrant that faces slower gas velocity (i.e. NE zone) produced a rougher surface and the quadrant that encounter faster gas velocity (i.e. SW zone) created a smoother surface. Therefore, the internal gas flow can be considered as one of the major influencing factors on the surface conditions of AM parts, which subsequently affects their fatigue behavior.

Conclusions

This study investigated the location dependency of SR parameters of 316L SS fabricated using Renishaw AM 250 system. The findings of this study can be summarized as below:

- With the statistical analysis of data in this study, based on one-way ANOVA and Kruskal-Wallis test, there is enough evidence to reject the null, i.e., a significant amount of surface roughness variation exists in different locations of the build platform.
- Here, from this statistical analysis of surface roughness characterization of additive manufactured parts, it is clear that NE specimens manufactured by Renishaw parts have significantly higher surface roughness compared to the other locations.

- Fatigue behavior of 316L SS parts well correlates with the surface roughness variation result obtained by the statistical approach.

Acknowledgement

This material is based upon work supported by the National Institute of Standards and Technology (NIST) under Grant No. 70NANB18H220.

References

[1] Yadollahi A, Shamsaei N. Additive manufacturing of fatigue resistant materials: Challenges and opportunities. Int J Fatigue 2017;98:14–31. https://doi.org/10.1016/j.ijfatigue.2017.01.001.

[2] Günther J, Leuders S, Koppa P, Tröster T, Henkel S, Biermann H, et al. On the effect of internal channels and surface roughness on the high-cycle fatigue performance of Ti-6Al-4V processed by SLM. Mater Des 2018;143:1–11. https://doi.org/10.1016/j.matdes.2018.01.042.

[3] Chen Y, Vastola G, Zhang YW. Optimization of Inert Gas Flow inside Laser Powder-Bed Fusion Chamber with Computational Fluid Dynamics. 29th Annu Int Solid Free Fabr Symp – An Addit Manuf Conf 2018:1931–9.

[4] A Comparison of Endosseous Dental Implant Surfaces - Cochran - 1999 - Journal of Periodontology - Wiley Online Library n.d.

[5] LoTzara RJ, MScD D, Testorf T, TrisI P, Weinstein RL. A Human Histologie Anaiysis of Osseotite and Machined Surfaces Using impiants with 2 Opposing Surfaces. n.d.

[6] Pegues J, Roach M, Scott Williamson R, Shamsaei N. Surface roughness effects on the fatigue strength of additively manufactured Ti-6Al-4V. Int J Fatigue 2018;116:543–52. https://doi.org/10.1016/j.ijfatigue.2018.07.013.

[7] Chen Z, Wu X, Tomus D, Davies CHJ. Surface roughness of Selective Laser Melted Ti-6Al-4V alloy components. Addit Manuf 2018;21:91–103. https://doi.org/10.1016/j.addma.2018.02.009.

[8] Wen P, Qin Y, Chen Y, Voshage M, Jauer L, Poprawe R, et al. Laser additive manufacturing of Zn porous scaffolds: Shielding gas flow, surface quality and densification. J Mater Sci Technol 2019;35:368–76. https://doi.org/10.1016/j.jmst.2018.09.065.

[9] Parteli EJR, Pöschel T. Particle-based simulation of powder application in additive manufacturing. Powder Technol 2016;288:96–102. https://doi.org/10.1016/j.powtec.2015.10.035.

[10] ASTM International. ASTM E466 Standard Practice for Conducting Force Controlled Constant Amplitude Axial Fatigue Tests of Metallic Materials. West Conshohocken, PA 2002:1–6. https://doi.org/10.1520/E0466-07.2.

[11] Iso. BS EN ISO 9001:2008. 2008.

[12] Frazier WE. Metal additive manufacturing: A review. J Mater Eng Perform 2014;23:1917–28. https://doi.org/10.1007/s11665-014-0958-z.

[13] Townsend A, Senin N, Blunt L, Leach RK, Taylor JS. Surface texture metrology for metal additive manufacturing: a review. Precis Eng 2016;46:34–47. https://doi.org/10.1016/j.precisioneng.2016.06.001.

[14] Lee S, Pegues J, Shamsaei N. Fatigue Behavior and Modeling for Additive Manufactured 304L Stainless Steel: The effect of Surface Roughness. Int J Fatigue 2020;141:105856. https://doi.org/10.1016/j.ijfatigue.2020.105856.

[15] Whip B, Sheridan L, Gockel J. The effect of primary processing parameters on surface roughness in laser powder bed additive manufacturing. Int J Adv Manuf Technol 2019;103:4411–22. https://doi.org/10.1007/s00170-019-03716-z.